# Cross-Energy Couplings from Magnetosonic Waves to Electromagnetic Ion Cyclotron Waves through Cold Ion Heating inside the Plasmasphere

Kazushi Asamura,[1] Masafumi Shoji,[2] Yoshizumi Miyoshi,[2] Yoshiya Kasahara,[3] Yasumasa Kasaba,[4] Atsushi Kumamoto,[4] Fuminori Tsuchiya,[4] Shoya Matsuda,[3] Ayako Matsuoka,[5] Mariko Teramoto,[6] Yoichi Kazama,[7] and Iku Shinohara[1]

[1]*Institute of Space and Astronautical Science, Japan Aerospace Exploration Agency, Sagamihara, Kanagawa 252-5210, Japan*
[2]*Institute for Space-Earth Environmental Research, Nagoya University, Nagoya, Aichi 464-8601, Japan*
[3]*Graduate School of Natural Science and Technology, Kanazawa University, Kanazawa, Ishikawa 920-1192, Japan*
[4]*Graduate School of Science, Tohoku University, Sendai, Miyagi 980-8578, Japan*
[5]*Graduate School of Science, Kyoto University, Kyoto 606-8502, Japan*
[6]*Graduate School of Engineering, Kyushu Institute of Technology, Kitakyushu, Fukuoka 804-8550, Japan*
[7]*Institute of Astronomy and Astrophysics, Academia Sinica, Taipei 10617, Taiwan*

(Received 9 July 2021; revised 6 October 2021; accepted 2 November 2021; published 10 December 2021)

Using a novel wave-particle interaction analysis, we show observational evidence of energy transfer from fast magnetosonic waves (MSWs) to low-energy protons in the magnetosphere. The analysis clearly indicates that the transferred proton energies are further converted to excite electromagnetic ion cyclotron waves. Since MSWs are excited by hot ions, cross-energy coupling of ions occurs through MSWs. The result also suggests a new energy transfer path of exciting electromagnetic ion cyclotron waves in the magnetosphere, and a complex interplay between various wave modes and particle populations.

DOI: 10.1103/PhysRevLett.127.245101

*Introduction.*—Fast magnetosonic waves (MSWs) are right-hand polarized compressional electromagnetic emissions above the local proton cyclotron frequency commonly observed in the terrestrial magnetosphere. These emissions are also known as equatorial noise or ion Bernstein waves and are mostly detected within a few degrees of the geomagnetic equator in the latitudinal direction [1–5]. Fast magnetosonic waves mainly have frequencies between the proton cyclotron frequency and the lower hybrid resonance frequency. They propagate with a highly oblique wave normal angle (WNA) near 90° [1,6]. The wave polarizes nearly normally, where the magnetic and electric field fluctuations are along the background magnetic field and wave vector, respectively [3,7,8]. Free energy for excitation of MSWs can be provided by a ringlike distribution of energetic protons, which is a positive gradient of phase space density in the perpendicular velocity distribution function at a velocity comparable to the local Alfvén speed [9–15].

Fast magnetosonic waves transfer energy to heat low-energy ions perpendicularly. Olsen [16] found a correspondence between MSWs and perpendicularly heated ions with energies less than a few hundred electron volts. Using the HOTRAY code, Horne *et al.* [11] showed that MSWs could heat low-energy protons transversely by energy absorption via cyclotron resonance. Through one-dimensional particle-in-cell simulations, Sun *et al.* [17] showed that the perpendicular heating of low-energy protons is likely caused by higher-order resonances with MSWs. Recently, based on the *in situ* satellite observations from the Van Allen Probes in plasmaspheric low-density regions, it was found that MSW activity co-occurred with the perpendicular heating of low-energy protons [18–20], $He^+$ [21], and $O^+$ [22] with energies less than a few hundred electron volts.

These anisotropic distributions of ions with energies of 10–100 eV potentially contribute to the generation of narrowband, high-frequency electromagnetic ion cyclotron (EMIC) waves [20], which are left-hand polarized waves below the local proton cyclotron frequency. Teng *et al.* [20] reported that the cyclotron resonance energy of EMIC waves just below the local proton cyclotron frequency ($\sim 0.92 f_{cp}$, where $f_{cp}$ is the proton cyclotron frequency) reached 10 eV in the inner magnetosphere, which is much lower than that for $\sim 0.45 f_{cp}$ corresponding to typical $H^+$-band EMIC waves ($0.25$–$0.5 f_{cp}$) [23,24]. This was calculated from the resonance condition and cold plasma dispersion relation using the data at the observation point, where the ion composition ratio was assumed to be the same as that in the energy range covered by the ion instrument (~1 eV–50 keV). Teng *et al.* [20] also showed that the observed frequency spectrum of the EMIC waves

 

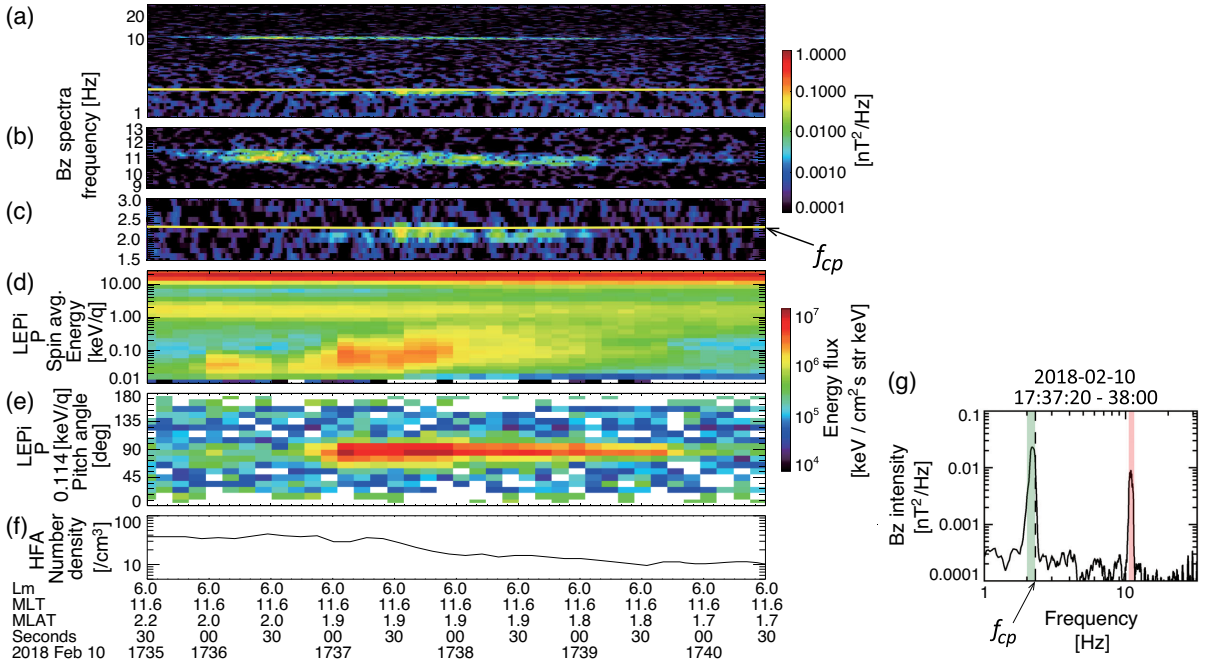


FIG. 1. Arase observations on February 10, 2018. (a)–(c) Dynamic spectra of wave magnetic energy in the spin axis direction of Arase. Solid yellow line indicates local proton cyclotron frequency. Panels (b) and (c) are magnified views of (a). (d) Energy spectra of omnidirectional proton energy fluxes. (e) Pitch angle distribution of proton energy fluxes at an energy of 114 eV. (f) Electron density profile calculated from the identified upper-hybrid resonance frequency using the observed frequency spectra of the wave electric field. (g) Power spectrum density of the spin axis component of the wave magnetic field. Red and green areas indicate frequency ranges of MSWs and EMIC waves, respectively, in the present study. Vertical dashed line in panel (g) indicates local proton cyclotron frequency (2.3 Hz).

agreed with the calculated linear growth rate based on the hot plasma dispersion relation.

Recently, wave-particle interaction analysis (WPIA) [25] has been applied to investigate the energy transfer between plasma waves and particles. The WPIA method calculates the inner product of the wave electric field vector ($\boldsymbol{E}$) and particle velocity vector ($\boldsymbol{v}$), multiplies by the particle charge ($q$), and then sums ($W_{Eint}$) in velocity space. A positive $W_{Eint}$ corresponds to the Joule heating of particles by plasma waves, whereas a negative $W_{Eint}$ indicates wave growth due to particles. Application of the WPIA method to *in situ* observation data of plasma particles and waves provides direct evidence of energy transfer between them. It is found that wave growth and frequency drift of EMIC waves in the inner magnetosphere occurred with negative $W_{Eint}$ [26]. Another study [27] showed the growth of EMIC waves by hot protons and subsequent energization of helium ions due to the generated EMIC waves in the outer magnetosphere. Recently, energy transfer between electrons and turbulent electric fields were measured using a similar technique in the magnetosheath [28]. More recently, we [29] identified the flux enhancement of protons moving in antiphase with a wave electric field vector associated with the growth of the EMIC falling tone. This is observational evidence of EMIC wave growth due to cyclotron trapping of particles, as predicted by the nonlinear wave growth theory [30–32]. There are also several simulation-based works using similar techniques [33]. However, these studies have not applied the WPIA method to MSWs in space plasma.

In the present Letter, we study an event in which an MSW was observed simultaneously with both perpendicularly heated low-energy ions and EMIC waves in the inner magnetosphere. We applied the WPIA method to the MSW for the first time to obtain direct evidence of energy transfer between the MSW and low-energy ions. Additionally, the WPIA method was applied to the EMIC waves to investigate the cross-energy coupling between them and MSWs through the heating of low-energy ions.

*Observations.*—The flux enhanced in the perpendicular component of low-energy ions simultaneously with MSW and EMIC wave activities was detected by Arase on February 10, 2018 [34]. Figure 1(a) shows the dynamic spectrum of the wave magnetic energy in the spin axis direction of Arase. Wave energy increased at 11 Hz from 17:35:30 to 17:39:30 UT. This wave was identified as an MSW because the polarization was near zero and the WNA approached 90° based on the Means method [44]. One minute after the MSW activity started, a narrow band enhancement of wave energy appeared just below $f_{cp}$ (2.3 Hz), as indicated by the yellow line. This wave was identified as an EMIC wave, as it was left-hand polarized and propagated with a small WNA (<30°), based on the Means method. Note that statistical studies show the

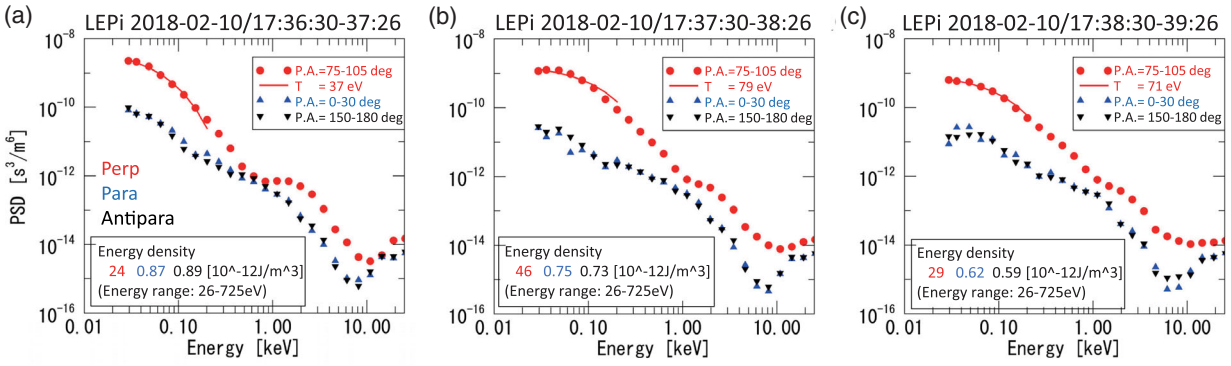


FIG. 2. Proton velocity distribution functions. Red, blue, and black colors indicate perpendicular (pitch angles within $90° \pm 15°$), parallel ($<30°$), and antiparallel ($>150°$) components, respectively. The data are averaged over 56 s, corresponding to seven satellite spins. Solid red lines show fitted lines of the perpendicular component using a nonlinear least-squares fitting method with Maxwellian distributions, where particle energies from 26 to 230 eV are considered. Perpendicular temperature ($T$) indicated in a box at the upper right in each panel was calculated by Maxwellian fitting. Energy density is for protons with energies between 26 and 725 eV.

average peak frequency of $H^+$-band EMIC waves is between 0.25 and $0.5 f_{cp}$ [23,24]. However, narrowband EMIC waves approaching $f_{cp}$ have been found simultaneously with MSW activity and perpendicular heating of 10–100 eV protons [20].

Figure 1(d) shows the observed energy spectra of omnidirectional proton energy fluxes. At 17:36 UT, proton energy fluxes began to increase at energies of 20–100 eV. The uppermost energy of the enhanced component gradually increased up to ~1 keV and lasted until 17:40 UT. The pitch angle spectra of proton fluxes at an energy of 114 eV are shown in Fig. 1(e). The flux enhancement is clearly concentrated around a pitch angle of 90°. The period of low-energy proton flux enhancement was closely correlated with the MSW and EMIC wave activity periods. The correlation between the MSW activity and the heating of low-energy protons in the perpendicular direction is consistent with previous numerical simulations [11,17]. Figure 1(f) shows the number density of ambient plasmas, calculated from the identified upper-hybrid resonance frequency. The number density gradually decreases to 20 $cm^{-3}$, although Arase was on its inbound pass (moving toward the Earth) during the observation period. Investigation of longer scale variations of the density showed that the event occurred in the plasmaspheric plume [34].

The evolution of the velocity distribution functions of protons for the perpendicular and field-aligned components is shown in Fig. 2. The phase space densities (PSDs) of the perpendicular components were greater than those of the field-aligned components throughout the event period. Assuming a gyrotropic distribution of PSDs, the temperatures of protons were estimated from PSDs by a nonlinear least-squares fitting method with Maxwellian distributions, where particle energies from 26 to 230 eV were considered. The perpendicular temperature increased up to 79 eV at 17:38 UT but then decreased. The energy densities of protons were also estimated with PSDs, and again, the gyrotropic distribution of the PSDs was assumed. The energy density in the perpendicular component (pitch angles within $90° \pm 15°$) and between 26 and 725 eV also increased and peaked at $4.6 \times 10^{-11}$ $J/m^3$ at 17:38 UT, whereas the field-aligned components were almost constant. These enhancements of perpendicular temperature and energy density indicate either possible energy transfer from plasma waves to particles through wave-particle interactions or transportation of plasmas from neighboring regions to the observation location.

*WPIA analysis.*—For the calculation of $W_{Eint}$ (energy transfer rate) with low-energy protons [34], we selected protons with energies ranging from 26 to 725 eV. Because the protons are perpendicularly heated, we further selected them by pitch angles within $90° \pm 15°$. Figure 3(a) shows the calculated $W_{Eint}$ for the observed MSW activity, where a frequency range between 10.5 and 11.5 Hz was selected for the calculation. $W_{Eint}$ was mostly positive from 17:35:50 to 17:39:20 UT, which coincided with the enhancement period of the MSW activity and the low-energy ion fluxes. A positive $W_{Eint}$ indicates that the MSWs gave their energies to low-energy protons. However, at around 17:37:20 UT, $W_{Eint}$ was negative. Having evaluated the resonance energy based on the cold plasma dispersion relation, we found that protons with energies above 500 eV can resonate with the observed MSWs which were fifth order harmonics of $f_{cp}$ [34]. Therefore, it is natural to consider that MSWs can sometimes gain energy from the ion populations with energies greater than 500 eV. Moreover, ion heating by MSWs likely occurs through cyclotron resonance above 500 eV, and nonresonant heating at lower energies [45].

Energy conservation law for plasma waves is given as

$$\frac{\partial}{\partial t}\left(\frac{1}{2}\varepsilon E^2 + \frac{1}{2\mu}B^2\right) + \boldsymbol{E}\cdot\boldsymbol{J} + \nabla\cdot\boldsymbol{S} = 0, \qquad (1)$$

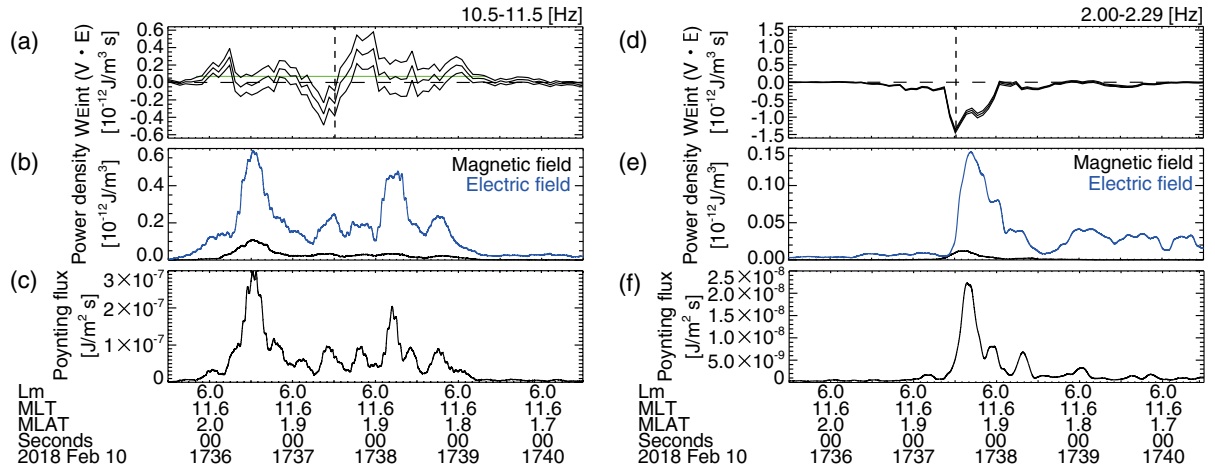


FIG. 3. Results of the WPIA calculations for the observed MSW activity. (a),(d) $W_{Eint}$. Three solid lines indicate calculated values and confidence intervals [26]. Vertical dashed lines indicate a period of negative peak of $W_{Eint}$ in panel (d). Green horizontal line in panel (a) indicates averaged value between 17:35:50 and 13:39:20 UT. (b),(e) Energy density of wave magnetic field (black) and electric field (blue). (c),(f) Poynting flux. For the WPIA calculations, the following selection criteria were applied: (1) frequency range between 10.5 and 11.5 Hz for panels (a)–(c), and that between 2.00 and 2.29 Hz for panels (d)–(f); (2) proton energies from 26 to 725 eV; and (3) pitch angles of protons within $90° \pm 15°$. In addition, a running average with an interval of 32 s for every 4 s was applied to the observed data.

where $t$, $B$, $J$, $S$, $\varepsilon$, and $\mu$ are the time, wave magnetic field vector, current vector, Poynting vector, permittivity of waves, and permeability of waves, respectively. From Fig. 3(a), $W_{Eint}$ from MSWs to protons was $6.5 \times 10^{-14}$ J/m$^3$ s on average in the period between 17:35:50 and 17:39:20 UT. $W_{Eint}$ corresponds to the third term of Eq. (1) because electrons do not resonate with MSWs and EMIC waves; only ions contribute to the resonance current through inhomogeneity in the velocity space [30]. The magnetic energy density ($B^2/2\mu$) and electric energy density ($\varepsilon E^2/2$) in the frequency range of MSWs (10.5–11.5 Hz) were $2.9 \times 10^{-14}$ J/m$^3$ and $2.1 \times 10^{-13}$ J/m$^3$, respectively, on average [Fig. 3(b)], where $\varepsilon$ was estimated based on phase velocity of MSWs derived from dispersion relation of cold plasma. Here, we assumed the typical ion composition ratio ($H^+$: 77%, $He^+$: 20%, $O^+$: 3%) in the plasmasphere [46]. The electromagnetic energy density of MSWs is not sufficient to supply $W_{Eint}$ by itself, as the event period is clearly longer than 10 s. We then considered the contribution of the Poynting flux. Based on Fig. 3(c), the averaged Poynting flux was $7.1 \times 10^{-8}$ J/m$^2$ s. The divergence of the Poynting flux is necessary to evaluate Eq. (1), which is difficult with single satellite observations. If we assume a uniform $W_{Eint}$ along the wave propagation path without any other energy inputs, the damping scale was 1100 km ($=7.1 \times 10^{-8}/6.5 \times 10^{-14}$ m) away from the observation location. Note that it is not always necessary for particles to receive and consume the energy at exactly the same time and location, because waves are propagating from other $L$ shells and particles are also drifting.

For the subsequent WPIA, we selected a frequency range of 2.00–2.29 Hz for the observed EMIC waves. Figure 3(d) shows the results of the WPIA calculations for the EMIC waves. $W_{Eint}$ is negative throughout the event period with a clear enhancement from 17:37:20 to 17:38:00 UT, where $W_{Eint}$ is $-7.7 \times 10^{-13}$ J/m$^3$ s, on average. This enhancement coincides with enhancements of the magnetic energy density and Poynting flux [Figs. 3(e) and 3(f)]. Since negative $W_{Eint}$ represents energy transfer from plasma

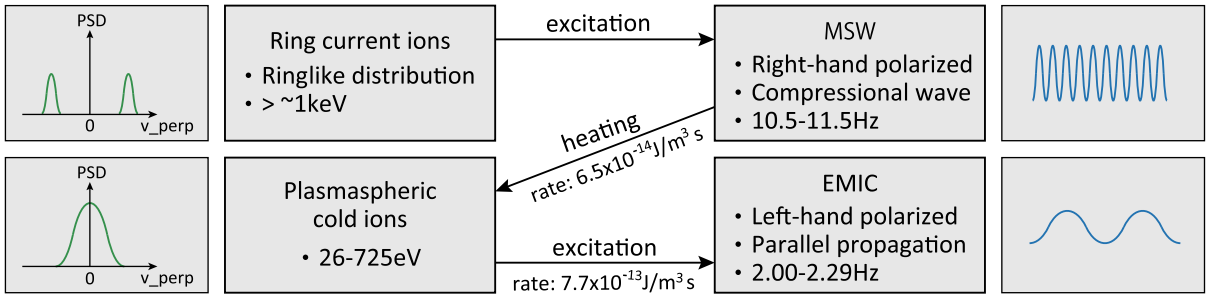


FIG. 4. Sketch of the cross-energy coupling process shown by this study. Arrows indicate the direction of energy transfer. v_perp indicates a perpendicular component of ion velocities.

particles to waves, the result indicates that the heated low-energy protons contributed to the growth of the EMIC waves, which is consistent with a previous study on EMIC waves with frequencies approaching $f_{cp}$ [20].

*Discussion.*—In the inner magnetosphere, MSWs can be excited by a ringlike distribution of energetic protons with velocities comparable to the local Alfvén speed [12]. The ringlike distributions can be formed by injections of plasma sheet ions or an energy-dependent drift of ions in the inner magnetosphere [47,48]. Our results suggest that the plasma sheet and ring current ions transfer some energy to the low-energy ions through excitation and damping of MSWs in the inner magnetosphere. Furthermore, a portion of the transferred energy is then converted to excite EMIC waves (Fig. 4). Therefore, this study shows a new cross-energy coupling process via multi-wave-particle interactions [49], in which MSWs work as a mediating agent for energy transfer. Such cross-energy coupling is important for the heating of plasmaspheric plasmas and contributes to the generation of EMIC waves and the nonthermal population of the inner magnetosphere, such as ion cloaks [50].

Previous ray-tracing studies in a cold plasma using the HOTRAY code show the possibility of linear mode conversion from MSWs to $H^+$-band EMIC waves at a location where the wave frequency is equal to the crossover frequency [51] and WNA is zero [52]. Multi-ion plasma also contributes to the mode conversion from MSWs to EMIC waves [5]. Thus, our results also show the existence of a new origin of EMIC waves of the space plasma through the heating of low-energy ions by MSWs. Furthermore, MSWs are known to energize electrons of hundreds of keV [53] and EMIC waves can cause sudden dropouts of MeV electron flux [54,55]. The connection between MSWs and EMIC wave generation may contribute to the transient dynamics of relativistic electrons in the inner magnetosphere. The present results highlight the complex interplay between various wave modes and particle populations in the magnetosphere.

In the fusion plasma, it has been observed that the geodesic acoustic mode (GAM) is excited when a frequency of energetic-particle driven GAM (EGAM) reaches twice the GAM frequency in a large helical device experiment [56]. Furthermore, numerical simulations have shown that GAM is excited by energetic particles that resonate with EGAM [57]. This phenomenon indicates energy transfer from EGAM to GAM through those energetic particles. Our results show similar energy transfer processes by directly evaluating the energy transfer rate in the space plasma, and thus, a similar approach may be applicable to the fusion plasma.

The data used in this study are ORB L2 v03 [58], LEP-i L2 3-D flux v03_00 [59], PWE/EFD L2 electric field waveform data v01_01 [60], PWE/HFA L3 electron density data v01_01 [61], MGF L2 high-resolution (64 Hz) magnetic field data v03_04 [62], and MGF L2 spin-averaged magnetic field data v03_04 [63]. Science data from the Arase satellite was obtained from the ERG Science Center [64] operated by ISAS/JAXA and ISEE/Nagoya University [64].

This work was supported by the Japan Society for the Promotion of Science (JSPS), KAKENHI Grants No. 17H06140, No. 20H01959, No. 20K14546 and No. 21H04526.

[1] C. T. Russel, R. E. Holzer, and E. J. Smith, OGO 3 observations of ELF noise in the magnetosphere: 2. The nature of the equatorial noise, J. Geophys. Res. **75**, 755 (1970).
[2] Y. Kasahara, H. Kenmochi, and I. Kimura, Propagation characteristics of the ELF emissions observed by the satellite Akebono in the magnetic equatorial region, Radio Sci. **29**, 751 (1994).
[3] O. Santolík, J. S. Pickett, D. A. Gurnett, M. Maksimovie, and N. Comilleau-Wehrlin, Spatiotemporal variability and propagation of equatorial noise observed by Cluster, J. Geophys. Res. **107**, 1495 (2002).
[4] N. P. Meredith, R. B. Horne, and R. R. Anderson, Survey of magnetosonic waves and proton ring distributions in the Earth's inner magnetosphere, J. Geophys. Res. **113**, A06213 (2008).
[5] Y. Miyoshi, S. Matsuda, S. Kurita, K. Nomura, K. Keika, M. Shoji, N. Kitamura, Y. Kasahara, A. Matsuoka, I. Shinohara, K. Shiokawa, S. Machida, O. Santolik, S. A. Boardsen, R. B. Horne, and J. F. Wygant, EMIC waves converted from equatorial noise due to $M/Q = 2$ ions in the plasmasphere: Observations from Van Allen Probes and Arase, Geophys. Res. Lett. **46**, 5662 (2019).
[6] S. Perraut, R. Gendrin, P. Robert, A. Roux, C. de Villedary, and D. Jones, ULF waves observed with magnetic and electric sensors on GEOS-1, Space Sci. Rev. **22**, 347 (1978).
[7] H. Laakso, H. Junginger, A. Roux, R. Schmidt, and C. de Villedary, Magnetosonic waves above $f_c(H^+)$ at geostationary orbit: GEOS 2 results, J. Geophys. Res. **95**, 10609 (1990).
[8] S. A. Boardsen, D. L. Gallagher, D. A. Gurnett, W. K. Peterson, and J. L. Green, Funnel-shaped, low-frequency equatorial waves, J. Geophys. Res. **97**, 14967 (1992).
[9] S. A. Curtis and C. S. Wu, Gyroharmonic emissions induced by energetic ions in the equatorial plasmasphere, J. Geophys. Res. **84**, 2597 (1979).
[10] S. Perraut, A. Roux, P. Robert, R. Gendrin, J.-A. Sauvaud, J.-M. Bosqued, G. Kremser, and A. Korth, A systematic study of ULF waves above $F_H^+$ from GEOS 1 and 2 measurements and their relationships with proton ring distributions, J. Geophys. Res. **87**, 6219 (1982).
[11] R. B. Horne, G. V. Wheeler, and H. S. C. K. Alleyne, Proton and electron heating by radially propagating fast magnetosonic waves, J. Geophys. Res. **105**, 27597 (2000).
[12] L. Chen, R. M. Thorne, V. K. Jordanova, and R. B. Horne, Global simulation of magnetosonic wave instability in the storm time magnetosphere, J. Geophys. Res. **115**, A11222 (2010).

[13] J. Sun, X. Gao, L. Chen, Q. Lu, X. Tao, and S. Wang, A parametric study for the generation of ion Bernstein modes from a discrete spectrum to a continuous one in the inner magnetosphere. I. Linear theory, Phys. Plasmas **23**, 022901 (2016).

[14] J. Sun, X. Gao, Q. Lu, L. Chen, X. Tao, and S. Wang, A parametric study for the generation of ion Bernstein modes from a discrete spectrum to a continuous one in the inner magnetosphere. II. Particle-in-cell simulations, Phys. Plasmas **23**, 022902 (2016).

[15] K. Min, K. Liu, R. E. Denton, F. Němec, S. A. Boardsen, and Y. Miyoshi, Two-dimensional hybrid particle-in-cell simulations of magnetosonic waves in the dipole magnetic field: On a constant *L*-shell, J. Geophys. Res. **125**, e2020JA028414 (2020).

[16] R. C. Olsen, Equatorially trapped plasma populations, J. Geophys. Res. **86**, 11235 (1981).

[17] J. Sun, X. Gao, Q. Lu, L. Chen, X. Liu, X. Wang, X. Tao, and S. Wang, Spectral properties and associated plasma energization by magnetosonic waves in the Earth's magnetosphere: Particle-in-cell simulations, J. Geophys. Res. **122**, 5377 (2017).

[18] K. Min, K. Liu, X. Wang, L. Chen, and R. E. Denton, Fast magnetosonic waves observed by Van Allen Probes: Testing local wave excitation mechanism, J. Geophys. Res. **123**, 497 (2018).

[19] Q. Ma, W. Li, C. Yue, R. M. Thorne, J. Bortnik, C. A. Kletzing, W. S. Kurth, G. B. Hospodarsky, G. D. Reeves, and H. E. Spence, Ion heating by electromagnetic ion cyclotron waves and magnetosonic waves in the Earth's inner magnetosphere, Geophys. Res. Lett. **46**, 6258 (2019).

[20] S. Teng, W. Li, X. Tao, Q. Ma, Y. Wu, L. Capannolo, X.-C. Shen, and L. Gan, Generation and characteristics of unusual high frequency EMIC waves, Geophys. Res. Lett. **46**, 14230 (2019).

[21] Z. Yuan, X. Yu, S. Huang, Z. Qiao, F. Yao, and H. O. Funsten, Cold ion heating by magnetosonic waves in a density cavity of the plasmasphere, J. Geophys. Res. **123**, 1242 (2018).

[22] S. Hill, N. Buzulukova, S. Boardsen, and M.-C. Fok, Local heating of oxygen ions in the presence of magnetosonic waves: Possible source for the warm plasma cloak?, J. Geophys. Res. **125**, e2019JA027210 (2020).

[23] N. P. Meredith, R. B. Horne, T. Kersten, B. J. Fraser, and R. S. Grew, Global morphology and spectral properties of EMIC waves derived from CRRES observations, J. Geophys. Res. **119**, 5328 (2014).

[24] X.-J. Zhang, W. Li, R. M. Thorne, V. Angelopoulos, J. Bortnik, C. A. Kletzing, W. S. Kurth, and G. B. Hospodarsky, Statistical distribution of EMIC wave spectra: Observations from Van Allen Probes, Geophys. Res. Lett. **43**, 12348 (2016).

[25] Y. Katoh, M. Kitahara, H. Kojima, Y. Omura, S. Kasahara, M. Hirahara, Y. Miyoshi, K. Seki, K. Asamura, T. Takashima, and T. Ono, Significance of wave-particle interaction Analyzer for direct measurements of nonlinear wave-particle interactions, Ann. Geophys. **31**, 503 (2013).

[26] M. Shoji, Y. Miyoshi, Y. Katoh, K. Keika, V. Angelopoulos, S. Kasahara, K. Asamura, S. Nakamura, and Y. Omura, Ion hole formation and nonlinear generation of electromagnetic ion cyclotron waves: THEMIS observations, Geophys. Res. Lett. **44**, 8730 (2017).

[27] N. Kitamura, M. Kitahara, M. Shoji, Y. Miyoshi, H. Hasegawa, S. Nakamura, Y. Katoh, Y. Saito, S. Yokota, D. J. Gershman, A. F. Vinas, B. L. Giles, T. E. Moore, W. R. Paterson, C. J. Pollock, C. T. Russell, R. J. Strangeway, S. A. Fuselier, and J. L. Burch, Direct measurements of two-way wave-particle energy transfer in a collisionless space plasma, Science **361**, 1000 (2018).

[28] C. H. K. Chen, K. G. Klein, and G. G. Howes, Evidence for electron Landau damping in space plasma turbulence, Nat. Commun. **10**, 740 (2019).

[29] M. Shoji, Y. Miyoshi, L. M. Kistler, K. Asamura, A. Matsuoka, Y. Kasaba, S. Matsuda, Y. Kasahara, and I. Shinohara, Discovery of proton hill in the phase space during interactions between ions and electro-magnetic ion cyclotron waves, Sci. Rep. **11**, 13480 (2021).

[30] Y. Omura, J. Pickett, B. Grison, O. Santolik, I. Dandouras, M. Engebretson, P. M. E. Décréau, and A. Masson, Theory and observation of electromagnetic ion cyclotron triggered emissions in the magnetosphere, J. Geophys. Res. **115**, A07234 (2010).

[31] M. Shoji and Y. Omura, Triggering process of electromagnetic ion cyclotron rising tone emissions in the inner magnetosphere, J. Geophys. Res. **118**, 5553 (2013).

[32] M. Shoji and Y. Omura, Nonlinear generation mechanism of EMIC falling tone emissions, J. Geophys. Res. **122**, 9924 (2017).

[33] J. Juno, G. G. Howes, J. M. TenBarge, L. B. Wilson III, A. Spitkovsky, D. Caprioli, K. G. Klein, and A. Hakim, A field-particle correlation analysis of a perpendicular magnetized collisionless shock, J. Plasma Phys. **87**, 905870316 (2021).

[34] See Supplemental Material at http://link.aps.org/supplemental/10.1103/PhysRevLett.127.245101 for instruments providing the observed data; for variation of ambient plasma density; for calculation details and for resonance energies with the observed MSWs, which includes Refs. [35–43].

[35] K. Asamura, Y. Kazama, S. Yokota, S. Kasahara, and Y. Miyoshi, Low-energy particle experiments—ion mass analyzer (LEPi) onboard the ERG (Arase) satellite, Earth Planets Space **70**, 70 (2018).

[36] Y. Kasaba, K. Ishisaka, Y. Kasahara, T. Imachi, S. Yagitani, H. Kojima, S. Matsuda, M. Shoji, S. Kurita, T. Hori, A. Shinbori, M. Teramoto, Y. Miyoshi, T. Nakagawa, N. Takahashi, Y. Nishimura, A. Matsuoka, A. Kumamoto, F. Tsuchiya, and R. Nomura, Wire probe antenna (WPT) and electric field detector (EFD) of plasma wave experiment (PWE) aboard the Arase satellite: Specifications and initial evaluation results, Earth Planets Space **69**, 174 (2017).

[37] Y. Kasahara, Y. Kasaba, H. Kojima, S. Yagitani, K. Ishisaka, A. Kumamoto, F. Tsuchiya, M. Ozaki, S. Matsuda, T. Imachi, Y. Miyoshi, M. Hikishima, Y. Katoh, M. Ota, M. Shoji, A. Matsuoka, and I. Shinohara, The plasma wave experiment (PWE) on board the Arase (ERG) satellite, Earth Planets Space **70**, 86 (2018).

[38] A. Matsuoka, M. Teramoto, R. Nomura, M. Nosé, A. Fujimoto, Y. Tanaka, M. Shinohara, T. Nagatsuma, K. Shiokawa, Y. Obana, Y. Miyoshi, M. Mita, T. Takashima,

and I. Shinohara, The ARASE (ERG) magnetic field investigation, Earth Planets Space **70**, 43 (2018).

[39] A. Kumamoto, F. Tsuchiya, Y. Kasahara, Y. Kasaba, H. Kojima, S. Yagitani, K. Ishisaka, T. Imachi, M. Ozaki, S. Matsuda, M. Shoji, A. Matsuoka, Y. Katoh, Y. Miyoshi, and T. Obara, High frequency analyzer (HFA) of plasma wave experiment (PWE) onboard the Arase spacecraft, Earth Planets Space **70**, 82 (2018).

[40] O. Santolík, M. Parrot, and F. Lefeuvre, Singular value decomposition methods for wave propagation analysis, Radio Sci. **38**, 1010 (2003).

[41] U. Taubenschuss and O. Santolík, Wave polarization analyzed by singular value decomposition of the spectral matrix in the presence of noise, Surv. Geophys. **40**, 39 (2019).

[42] D. P. Hartley, C. A. Kletzing, O. Santolík, L. Chen, and R. B. Horne, Statistical properties of plasmaspheric hiss from Van Allen Probes observations, J. Geophys. Res. **123**, 2605 (2018).

[43] D. P. Hartley, C. A. Kletzing, L. Chen, R. B. Horne, and O. Santolík, Van Allen Probes observations of chorus wave vector orientations: Implications for the chorus-to-hiss mechanism, Geophys. Res. Lett. **46**, 2337 (2019).

[44] J. D. Means, Use of the three-dimensional covariance matrix in analyzing the polarization properties of plane waves, J. Geophys. Res. **77**, 5551 (1972).

[45] A. V. Artemyev, D. Mourenas, O. V. Agapitov, and L. Blum, Transverse eV ion heating by random electric field fluctuations in the plasmasphere, Phys. Plasmas **24**, 022903 (2017).

[46] V. K. Jordanova, J. Albert, and Y. Miyoshi, Relativistic electron precipitation by EMIC waves from self-consistent global simulations, J. Geophys. Res. **113**, A00A10 (2008).

[47] M. F. Thomsen, M. H. Denton, V. K. Jordanova, L. Chen, and R. M. Thorne, Free energy to drive equatorial magnetosonic wave instability at geosynchronous orbit, J. Geophys. Res. **116**, A08220 (2011).

[48] V. K. Jordanova, D. T. Welling, S. G. Zaharia, L. Chen, and R. M. Thorne, Modeling ring current ion and electron dynamics and plasma instabilities during a high-speed stream driven storm, J. Geophys. Res. **117**, A00L08 (2012).

[49] Y. Miyoshi, I. Shinohara, T. Takashima, K. Asamura, N. Higashio, T. Mitani, S. Kasahara, S. Yokota, Y. Kazama, S.-Y. Wang, S. W. Y. Tam, P. T. P. Ho, Y. Kasahara, Y. Kasaba, S. Yagitani, A. Matsuoka, H. Kojima, Y. Katoh, K. Shiokawa, and K. Seki, Geospace exploration project ERG, Earth Planets Space **70**, 101 (2018).

[50] C. R. Chappell, M. M. Huddleston, T. E. Moore, B. L. Giles, and D. C. Delcourt, Observations of the warm plasma cloak and an explanation of its formation in the magnetosphere, J. Geophys. Res. **113**, A09206 (2008).

[51] R. B. Horne and R. M. Thorne, On the preferred source location for the convective amplification of ion cyclotron waves, J. Geophys. Res. **98**, 9233 (1993).

[52] R. B. Horne and Y. Miyoshi, Propagation and linear mode conversion of magnetosonic and electromagnetic ion cyclotron waves in the radiation belts, Geophys. Res. Lett. **43**, 10034 (2016).

[53] D. Mourenas, A. V. Artemyev, O. V. Agapitov, and V. Krasnoselskikh, Analytical estimates of electron quasi-linear diffusion by fast magnetosonic waves, J. Geophys. Res. **118**, 3096 (2013).

[54] R. M. Thorne and C. F. Kennel, Relativistic electron precipitation during magnetic storm main phase, J. Geophys. Res. **76**, 4446 (1971).

[55] D. Mourenas, A. V. Artemyev, Q. Ma, O. V. Agapitov, and W. Li, Fast dropouts of multi-MeV electrons due to combined effects of EMIC and whistler mode waves, Geophys. Res. Lett. **43**, 4155 (2016).

[56] T. Ido, K. Itoh, M. Osakabe, M. Lesur, A. Shimizu, K. Ogawa, K. Toi, M. Nishiura, S. Kato, M. Sasaki, K. Ida, S. Inagaki, S.-I. Itoh, and the LHD Experiment Group, Strong Destabilization of Stable Modes with a Half-Frequency Associated with Chirping Geodesic Acoustic Modes in the Large Helical Device, Phys. Rev. Lett. **116**, 015002 (2016).

[57] H. Wang, Y. Todo, T. Ido, and Y. Suzuki, Chirping and Sudden Excitation of Energetic-Particle-Driven Geodesic Acoustic Modes in a Large Helical Device Experiment, Phys. Rev. Lett. **120**, 175001 (2018).

[58] Y. Miyoshi, I. Shinohara, and C.-W. Jun, The level-2 orbit data of exploration of energization and radiation in geospace (ERG) Arase satellite, ERG-Science Center v03 (2018) 10.34515/DATA.ERG-12000.

[59] K. Asamura, Y. Miyoshi, and I. Shinohara, The LEPi instrument level-2 3D flux data of exploration of energization and radiation in geospace (ERG) Arase satellite, ERG-Science Center v03_00 (2018) 10.34515/DATA.ERG-05000.

[60] Y. Kasahara, Y. Kasaba, S. Matsuda, M. Shoji, T. Nakagawa, K. Ishisaka, S. Nakamura, M. Kitahara, Y. Miyoshi, and I. Shinohara, The PWE/EFD instrument level-2 electric field waveform data of exploration of energization and radiation in geospace (ERG) Arase satellite, ERG-Science Center v01_01 (2020) 10.34515/DATA.-ERG-07003.

[61] Y. Kasahara, A. Kumamoto, F. Tsuchiya, H. Kojima, S. Matsuda, A. Matsuoka, M. Teramoto, M. Shoji, S. Nakamura, M. Kitahara, A. Maeda, Y. Miyoshi, and I. Shinohara, The PWE/HFA instrument level-3 electron density data of exploration of energization and radiation in geospace (ERG) Arase satellite, ERG-Science Center v01_01 (2021) 10.34515/DATA.ERG-10001.

[62] A. Matsuoka, M. Teramoto, S. Imajo, S. Kurita, Y. Miyoshi, and I. Shinohara, The MGF instrument level-2 high-resolution magnetic field data of exploration of energization and radiation in geospace (ERG) Arase satellite, ERG-Science Center v03_04 (2018) 10.34515/DATA.ERG-06000.

[63] A. Matsuoka, M. Teramoto, S. Imajo, S. Kurita, Y. Miyoshi, and I. Shinohara, The MGF instrument level-2 spin-averaged magnetic field data of exploration of energization and radiation in geospace (ERG) Arase satellite, ERG-Science Center v03_04 (2018) 10.34515/DATA.ERG-06001.

[64] Y. Miyoshi, T. Hori, M. Shoji, M. Teramoto, T. F. Chang, T. Segawa, N. Umemura, S. Matsuda, S. Kurita, K. Keika, Y. Miyashita, K. Seki, Y. Tanaka, N. Nishitani, S. Kasahara, S. Yokota, A. Matsuoka, Y. Kasahara, K. Asamura, T. Takashima, and I. Shinohara, The ERG science center, Earth Planets Space **70**, 96 (2018).